International Journal of New Developments in Engineering and Society
ISSN 2522-3488 Vol. 3, Issue 5: 88-96, DOI: 10.25236/IJNDES.2019.030510

Natural Convection and Oxygen Transfer of Liquid Lead-bismuth Eutectic in Cylindrical Container

Yungan Zhao[1], Fenglei Niu[2]

1 Beijing Key Laboratory of Passive Safety Technology for Nuclear Energy, North China Electric Power University, Beijing 102206, China
2 Beijing Key Laboratory of Passive Safety Technology for Nuclear Energy, North China Electric Power University, Beijing 102206, China

ABSTRACT. *The present study carries out numerical analysis of the coupled natural convection and oxygen transfer of liquid lead-bismuth eutectic (LBE) for calibrating low concentration level oxygen sensors. The analysis is performed on the 3-D cylindrical container, where the fluid in low Rayleigh number for the purpose of sensor calibration. The oxygen is supplied from the cover gas at the top of the container. Natural convection and oxygen transfer are examined under three temperature boundary conditions: (a) higher heated temperature in lower part and lower heated temperature in upper part of the sidewalls of the container; (b) higher heated temperature from the sidewalls and lower heated temperature from the top of the container; (c) higher heated temperature from one half side and lower heated temperature from the other. It is found that there are four, two and one convective circulation cells at the vertical section under conditions (a), (b), and (c), respectively. All these flows induced by the natural convection greatly enhance the oxygen transfer in the liquid metal. The most efficient one is under condition (b), it takes ~10^3s for the oxygen concentration in the whole field to reach ~90% of the input oxygen concentration from the top, instead of ~10^6 s by the pure diffusion.*

KEYWORDS: *Natural convection; Oxygen transfer;Lead-bismuth; Eutectic numerical simulation*

1. Introduction

Liquid lead and lead-bismuth eutectic (LBE) is being considered as a candidate for lead cooled fast reactor (LFR) coolant and spallation neutron targets in accelerator-driven transmutation systems (ADS) for its favourable thermal-physical, chemical and nuclear properties. These properties include high boiling temperature, low melting point, high thermal conductivity, low viscosity, low neutron capture and moderation, and high spallation neutron yield [1-3]. One of the main problems in using LBE is its adverse effect on structural materials. This liquid-metal dissolves many stainless steel alloying components that can lead to severe corrosion. [4] A

method to prevent corrosion in LBE systems is to create and maintain a protective oxide film on the surface of the stainless steel [5, 6]. Unfortunately, it has been found that the pre-oxidation of steels does not prevent corrosion through the oxygen exchange in non-isothermal lead and bismuth systems based on the thermodynamic consideration [7]. Instead, a well-controlled extremely low oxygen concentration level (as low as 2×10^{-7}~10^{-5}wt. % in liquid LBE at 400~600oC[8-10]) is crucial in avoiding the corrosion of lead-alloy carriers as well as in avoiding the formation of lead oxide contaminations. The proper formation of oxide layers critically depends on the control of oxygen concentration, so it is necessary to monitor the on-line concentration in LBE systems.

In order to measure oxygen concentration in liquid LBE under high temperature (up to 700^{o}C), an alumina-based solid electrolyte sensor is developed. The measurement range of this type of sensor is from a few hundreds of ppm to several tens of ppb in the case of using molten bismuth saturated with oxygen as the reference. However, the characteristics of the sensor have not been well examined at present. A stable, uniform and extremely low oxygen-concentration LBE environment needed to be established for the purpose of calibrating and testing the sensor. In fact, oxygen diffusivity in LBE is very low (~10^{-8}m^2/s at 500^{o}C)[11], so the enhancement of oxygen transfer is necessary in this oxygen sensor calibration system. Despite the fact that mechanical oscillation and stirring methods may be efficacious for producing a stable and uniform oxygen concentration, it is difficult to predict the time for oxygen reaching the expected level in the bulk of liquid LBE if using mechanical mixing methods. In order to design the new mixing apparatus, some numerically simulations of oxygen-mixing processes in a 3-D cylindrical container under different temperature conditions are done to study the natural convection mixing characteristics and estimate the time for concentration equilibrium.

In this paper, numerical analysis is carried out in a simplified cylindrical enclosure in which oxygen is induced from the top and is transferred into the LBE fluid by natural flow. The simplified geometry can be used to simulate the proposed natural-convection-enhanced oxygen transfer in the apparatus for oxygen sensor calibration, in which liquid LBE fills a space of cylindrical container and oxygen is introduced from the top by using a cover gas. The gap between the top wall of the container and the liquid surface is narrow, the temperature gradient in this space is negligible, and the gas-liquid LBE interface is considered as a free surface, which is assumed for the laminar liquid metal flow. Three different temperature boundary conditions are applied to create natural convection mixing. Finally, the critical time to reach the uniform oxygen concentration is determined for each temperature boundary condition.

2. Mathematical model and numerical method

A simplified 3-D geometry for our experimental setup of cylindrical container and the calculating domain is shown in Figure 1. On top of the cylindrical container, the gas oxygen is imported from an O_2/He gas cylinder. The liquid metal fills a

space of with diameter *D* and height *H*. The momentum and heat transports are described by the following continuity, momentum and energy equations with the Boussinesq approximation:

$$\nabla \cdot \vec{v} = 0 \tag{1}$$

$$\frac{\partial \vec{v}}{\partial t} + (\vec{v} \cdot \nabla)\vec{v} = -\frac{1}{\rho}\nabla p - \beta(T - T_0)\vec{g} + \frac{\mu}{\rho}\nabla^2 \vec{v} \tag{2}$$

$$\frac{\partial T}{\partial t} + (\vec{v} \cdot \nabla)T = -\alpha \nabla^2 T \tag{3}$$

Where $\vec{v}$ is the flow velocity vector; p is the pressure; T is the temperature of LBE; $\vec{g}$ is the vector of gravity acceleration; and β, ρ, μ and α are the thermal expansion coefficient, density, dynamic viscosity, and thermal diffusivity of LBE, respectively. T_0 is the reference of temperature that equals the lower temperature at the boundary, T_{low}, in the present study. Table 1. lists the values of these parameters for liquid LBE at 500^{o}C.

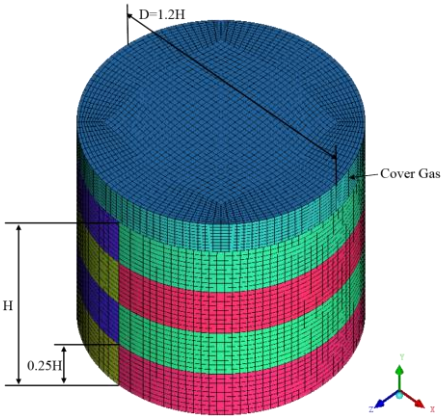

Figure. 1 3-D Schematic of Simplified Cylindrical Container/Calculating Domain

Table. 1 Properties of liquid LBE at 500oC[12]

Parameters	Values
Density ρ (kg/m^3)	1.012e4
Dynamic viscosity μ (kg/m-s)	1.376e-3
Kinetic viscosity ν (m^2/s)	1.360e-7
Thermal diffusivity α (m^2/s)	9.889e-6
Thermal expansion coefficient β (1/K)	1.302e-4
Thermal capacity Cp (kJ/kg-K)	146.5
Thermal conductivity K (W/m-K)	13.981

In order to describe the boundary conditions specifically, vertical sections of cylinder cut from the diameter are shown in Figure 2. Non-slip boundary conditions are applied on the sidewalls of the cylindrical container, while free surface condition is assumed at the interface of the cover gases and the liquid metal. Three different temperature boundary conditions are considered, as shown in Figure 2 (a)-(c) respectively, red area are higher temperature heater and blue area are lower one. Oxygen input is from the cover gases at the top of the container. At other boundaries without heaters, adiabatic conditions are satisfied.

Dimensionless velocity $U_c = \sqrt{\beta g D(T_{high} - T_{low})}$ (diameter D is assumed as characteristic length) is introduced and then dimensionless velocity vector:

$$\vec{V} = \frac{\vec{v}}{\sqrt{\beta g D(T_{high} - T_{low})}} \tag{4}$$

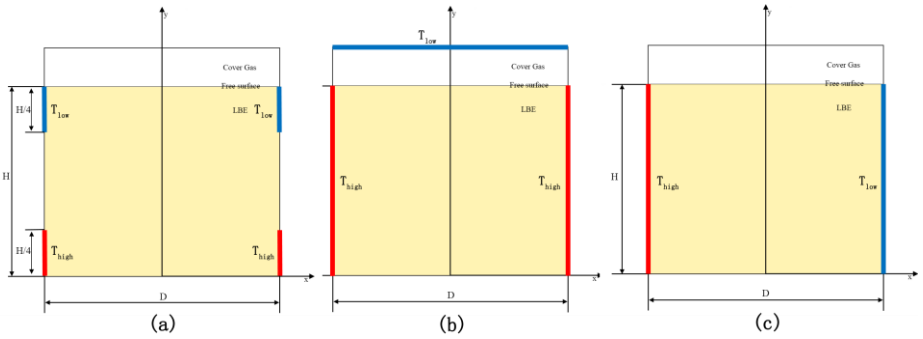

Figure. 2 Boundary Conditions Shown in Vertical Sections of Cylindrical Container

With dimensionless coordinates *X*, *Y*, *Z*: $X = \frac{2x}{D}$, $Y = \frac{y}{H}$, $Z = \frac{2z}{D}$, are introduced and then the dimensionless velocity boundary conditions can be expressed as follows:

$$\sqrt{X^2 + Z^2} = 1,\ 0 \le Y \le 1,\ U = V = W = 0 \tag{5}$$

$$Y = 0,\ 0 < \sqrt{X^2 + Z^2} \le 1,\ U = V = W = 0 \tag{6}$$

$$Y = 1,\ 0 < \sqrt{X^2 + Z^2} \le 1,\ V = 0,\ \frac{\partial U}{\partial Y} = \frac{\partial W}{\partial Y} = 0 \tag{7}$$

Without consideration the pressure field, the velocity field of the flow at the vertical section can be described by the vorticity equation for laminar and incompressible flows, which can be written as follows:

ISSN 2522-3488 Vol. 3, Issue 5: 88-96, DOI: 10.25236/IJNDES.2019.030510

$$\frac{\partial \vec{\omega}}{\partial t} + (\vec{v} \cdot \nabla)\vec{\omega} = \beta g \frac{\partial T}{\partial X} + \frac{\mu}{\rho} \nabla^2 \vec{\omega} \tag{8}$$

Where $\vec{\omega} = \nabla \times \vec{v}$ is the vorticity. In the vertical section and incompressible case, $\vec{\omega}$ can be expressed as $\vec{\omega} = -\left(\frac{\partial^2 \psi}{\partial x^2} + \frac{\partial^2 \psi}{\partial y^2} \right)$. Where Ψ is stream function and $u = \frac{\partial \psi}{\partial y}$, $v = -\frac{\partial \psi}{\partial x}$.

$$\text{With } U_c = \sqrt{\beta g D \Delta T},$$

$$t^* = \frac{t\sqrt{\beta g D (T_{high} - T_{low})}}{D} \tag{9}$$

$$\Omega = \frac{\vec{\omega} D}{\sqrt{\beta g D (T_{high} - T_{low})}} \tag{10}$$

Here t^*, Ω are time and voracity in dimensionless, respectively. dimensionless temperature $\Theta = \frac{T - T_{low}}{T_{high} - T_{low}}$ is assumed, and then the equations of vorticity and energy can be expressed in

dimensionless forms as follows:

$$\frac{\partial \Omega}{\partial t^*} + (\vec{V} \cdot \nabla)\Omega = \frac{\partial \Theta}{\partial X} + \frac{1}{\text{Re}} \nabla^2 \Omega \tag{11}$$

$$\frac{\partial \Theta}{\partial t^*} + (\vec{V} \cdot \nabla)\Theta = \frac{1}{\text{Re}\,\text{Pr}} \nabla^2 \Theta \tag{12}$$

Where $Ra = \frac{\rho D U_c}{\mu}$ is Reynolds number, and $\text{Pr} = \frac{\mu}{\rho \alpha}$ is Prandtl number.

The convection-diffusion equation for calculating the mass transport of oxygen can be expressed as:

$$\frac{\partial c}{\partial t} + (\vec{V} \cdot \nabla)c = -\nabla \vec{J} \tag{13}$$

Where c is oxygen concentration and $\vec{J} = \nabla dc$ (d is the oxygen diffusion coefficient) is the diffusion flux of oxygen. In the experiment, oxygen is introduced at the top of the container, so the oxygen concentration at the liquid surface can be assumed as a constant, which is obviously is the maximum concentration in the LBE

flow. Introduced dimensionless oxygen concentration $C = \frac{c}{c_{\max}}$, ($C_{\max} = 1$)Equation (13). can be expressed as:

$$\frac{\partial C}{\partial t} + (\vec{V} \cdot \nabla) C = \frac{1}{\mathrm{Re}\, Sc} \nabla^2 C \qquad (14)$$

where $Sc = \frac{\mu}{\rho d}$ is Schmidt number.

In order to verify the independency of meshes and time step, the calculations were repeated on 80000, 150000, 300000 meshes in the calculating domain. The dimensionless time steps of 1.0e-2, 5.0e-3, 1.0e-3, are selected for the mass transfer problem. Since negligible changes are shown on mass, flow and temperature distributions for different meshes and time steps, therefore, the results presented here are referred to 80000 meshes and the dimensionless time step of 1.0e-2 for mass transfer equation.

3. Result and analysis

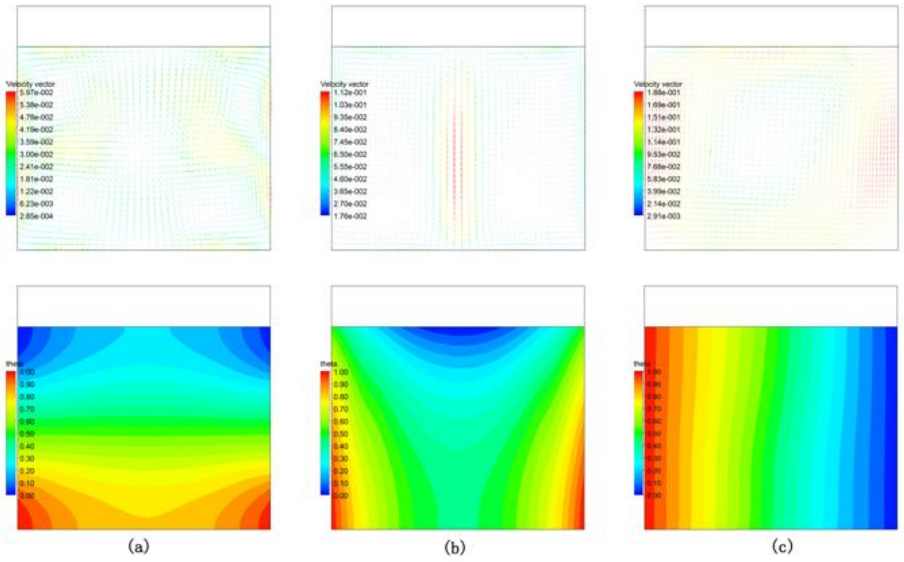

Figure.3 Velocity Field (upside panel) and Isotherms of the Convection Flow under Boundary Conditions (a), (b), and (c)

The steady-state velocity distributions and isotherms are shown in Figure 3. And the three temperature boundary conditions shown in Figure 2 at *Ra*= 60234.9 (corresponding to the values of β , ρ , μ , α for liquid LBE in Table 1. and

$\Delta T = T_{high} - T_{low} = 0.01^{o}C$, $D = 0.2m$). From the velocity vector plots, it can be found that there are four vortical cells in the vertical section for case (a) when the lower sidewall is higher temperature and the upper sidewall is lower temperature. There are two vortical cells for case (b) when the sidewall is higher temperature and the top wall is lower temperature. When one sidewall is high temperature and another sidewall is lower temperature, as in case (c), there is only one vortical cell in the container. The velocity vector represents the magnitude of the flow velocity as well as its direction at local positions. The flow directions at the interfaces between adjacent vortical cells are identical in cases (a) and (b). Vortical cells are separate by these virtual interfaces. For cases (a) and (b), although the convection inside the vortical cells is strong, the convection between vortical cells is weak. Higher flow velocity would result in more and quicker convective heat and mass transfer. For case (a), the maximal dimensionless velocity of the flow is 0.0597. For case (b), the maximal dimensionless flow velocity in the container is 0.1120, which is about twice as much as that in case (a). For case (c), the maximal dimensionless flow velocity in the container is 0.1880, which is the highest dimensionless velocity among three cases. This indicates that temperature boundary condition (c) is the most efficient way to enhance the flow convection, compared to conditions (a) and (b). As expected, in case (c), the fluid flows from the hotter wall to the colder wall in the upper part of the enclosure, while flows from the colder wall to the hotter wall at the lower part of the enclosure. Subsequently, the isotherm distributions are distorted due to the intensive convection flow.

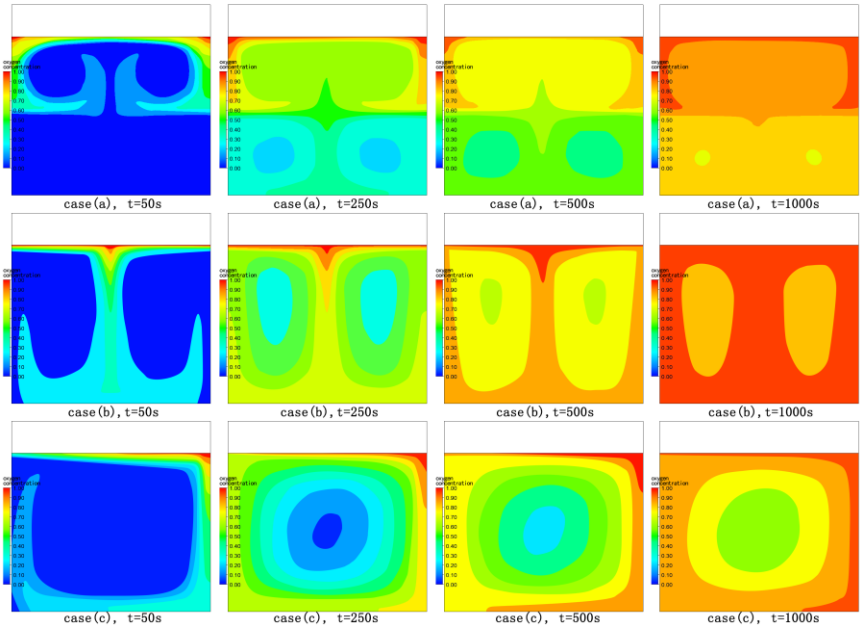

Figure.4 Concentration Contours at Different Times t=50s, 250s, 500s, and 1000s

Oxygen transport is studied under Rayleigh numbers *Ra*=60234.9 and Schmidt numbers *Sc*=13.6 (corresponding to the values of ν shown in Table 1 and oxygen diffusion coefficient *d*=1.0e-8 m^2/s). The instantaneous oxygen concentration distributions at several time moments (*t*= 50 s, 250 s, 500 s and 1000 s) are illustrated in Figure 4 for temperature boundary conditions in case (a), (b) and (c). These concentration contours clearly show that natural convection is the dominant driving force for oxygen transfer.

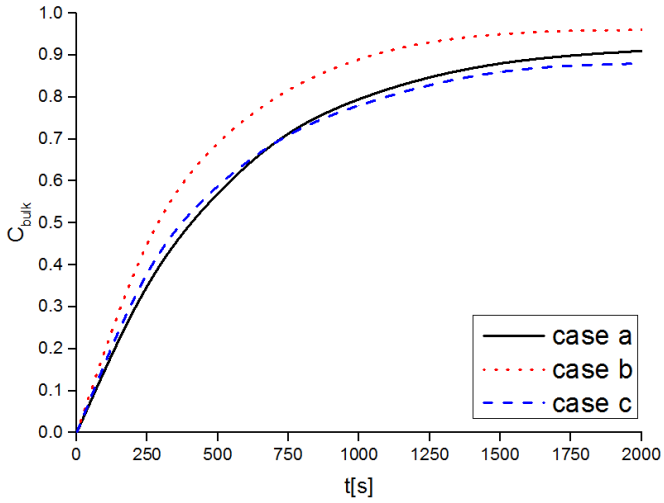

Figure.5 The Average Oxygen Concentration with Time for Case (a), (b), (c)

Figure 5. shows that under condition in case (b), it only takes about 1000 s for the oxygen to reach equilibrium at *Ra*= 60234.9 and *Sc*= 13.6, which is ~90% of the oxygen concentration from the cover gas. Under conditions in case (a) and (c), it will take longer time to reach the equilibrium. But all these times are much shorter than the characteristic pure diffusion time (~10^6 s).

5. Conclusion

The numerical analysis of the natural convection which driven oxygen transfer in the liquid LBE is presented in this work for three temperature boundary conditions. The results of simulation show that the natural convections induced by all the boundary conditions greatly enhance the oxygen transport in the liquid LBE. The most efficient one is under temperature condition (b), in which the sidewalls of the container are heated by higher temperature and the top wall is heated by lower temperature. It takes about 1000s for the oxygen concentration in the whole field to reach ~90% of the input concentration from the top.

Acknowledgements

This research is supported by the National Natural Science Foundation of China (Grant No. 11635005, 11705059) and the Fundamental Research Funds for the Central Universities (2018ZD10).

References

[1] Marino.A, Lim.J, Keijers.S, et al.(2018). Numerical modeling of oxygen mass transfer in a wire wrapped fuel assembly under flowing lead bismuth eutectic. J Nucl Mate, vol.506, pp.53-62.
[2] J.S.Zhang, N.Li(2008). Review of the studies on fundamental issues in LBE corrosion. J Nucl Mater, vol.373, no.1-3, pp.351-377.
[3] Lim.J, Manfredi.G, Gavrilov.S, et al(2014). Control of dissolved oxygen in liquid LBE by electrochemical oxygen pumping. Sensor Actuat B-Chem, vol.204, pp.388-392.
[4] Niu.FL, Candalino.R, Li.N(2007). Effect of oxygen on fouling behavior in lead-bismuth coolant systems. J Nucl Mater; vol.366, no.1-2, pp.216-222.
[5] Bassini.S, DiPiazza I, Antonelli.A, et al(2018). In-loop oxygen reduction in HLM thermal-hydraulic facility NACIE-UP. Prog Nucl Energ.no.105, pp.137-145.
[6] D.D.Li, Y.G.Zhang, H.Y.He, et al(2015). Dynamic process of H-controlled oxygen concentration in LBE: A first-principles study. J Nucl Mater, vol.467, pp.181-185.
[7] R.S. Lillard, C. Valot, M.A. Hill, et al(2003). The influence of pre-oxidation on the corrosion of steels in liquid lead bismuth eutectic. Los Alamos National Laboratory Report.
[8] L.Ning(2002). Active control of oxygen in molten lead–bismuth eutectic systems to prevent steel corrosion and coolant contamination. J Nucl Mater , vol.300, no.1, pp.73-81.
[9] Müller.G, Heinzel.A, Schumacher.G, et al(2003). Control of oxygen concentration in liquid lead and lead–bismuth. J Nucl Mater, vol.321, no.2-3, pp.256-262.
[10] Lambrinou.K, Charalampopoulou.E, Van der Donck.T(2017). Dissolution corrosion of 316L austenitic stainless steels in contact with static liquid lead-bismuth eutectic (LSE) at 500 degrees C. J Nucl Mater, vol.490, pp.9-27.
[11] H. Ma, P. Guo, J.S. Zhang, N.Li(2005). Enhancement of oxygen transfer in liquid lead and lead-bismuth eutectic by natural convection. Int J Heat Mass Tran, vol.48, no.13, pp.2601-2612.
[12] Agency.NE(2015). Handbook on Lead-bismuth Eutectic Alloy and Lead Properties. Materials Compatibility, Thermal-hydraulics and Technologies-Edition.